Effects of void deck on the airflow and pollutant dispersion in 3D street canyons

Chung Hyok Sin
University of Shanghai for Science and Technology
Yang Luo
University of Shanghai for Science and Technology
Kwang Song Jon
University of Shanghai for Science and Technology
Peng-Yi Cui
University of Shanghai for Science and Technology
Yuandong Huang (huangyd@usst.edu.cn)
University of Shanghai for Science and Technology

Research Article

Keywords: Airflow, CFD, Void deck, Street canyon, Traffic pollutant dispersion

Posted Date: April 25th, 2022

DOI: https://doi.org/10.21203/rs.3.rs-1533873/v1

Effects of void deck on the airflow and pollutant dispersion in 3D street canyons

Chung Hyok Sin[a,b], Yang Luo[a], Kwang Song Jon[a], Peng-Yi Cui[a], Yuan-dong Huang[a]*

[a]*School of Environment and Architecture, University of Shanghai for Science and Technology, Shanghai, 200093, China*

[b]*Natural Science Center, Kim Il Sung University, Taesong District, Pyongyang, Democratic People's Republic of Korea*

* Corresponding author, email: huangyd@usst.edu.cn;

Correspondence: School of Environment and Architecture, University of Shanghai for Science and Technology, No.516, Jungong Road, Yangpu District, Shanghai, China, 200093, Phone and Fax +86 021 55275611, email: huangyd@usst.edu.cn;

Abstract

In general, urban canyons are the areas most clearly affected by traffic pollutants since the ability of the canyon to self-ventilate is inhibited due to blockage of buildings or other urban structures. However, previous studies have aimed to improve the pedestrian-level wind speed with void deck in single buildings or short canyons. This study investigated the effects of void deck height and location, and building height on the airflow field and the traffic pollutant diffusion in a long canyon with *L/H=10*, validated by wind-tunnel experiment data. The results show that the void decks have a significant effect on the airflow and pollutant distribution inside the canyon. Air exchange rates (ACH) of the canyons with the void deck are much larger than that of regular canyons, and the perturbation changes of turbulence (ACH') decrease. When the void deck is at both buildings, the ACH is the highest, followed by the case where the void deck is at the leeward building. Also, for the canyons with the void deck, traffic pollutants are removed out of the canyon by the strong airflow through the void deck. Therefore, unlike the regular canyons, as the void deck and the building height increases, the strength of the airflow through the void deck becomes stronger, and as a result, the mean pollutant concentration is significantly reduced at both walls and the pedestrian respiration level. The mean pollutant concentration on the wall of the building with the void deck and on the pedestrian respiration plane close to it is near zero. These findings can help ease traffic pollution inside the street canyons composed of high-rise buildings, especially in tropical cities.

Keywords: Airflow; CFD; Void deck; Street canyon; Traffic pollutant dispersion

1. Introduction

Today's urban streets are becoming more and more high-density and high-rise (Zhang et al. 2018d). These compact urban structures form a unique urban climate and affect on the health of citizens (Chew and Norford 2018b). In particular, for the street canyons, since the wind speed is relatively low by the blocking effect of urban structures, the influence of vehicle exhaust on pedestrians and near-road residents is very large (Chen and Norford 2017a; Yim et al. 2010). Therefore, many studies have been conducted on airflow and pollutant dispersion inside the street canyons to reduce these adverse effect of traffic pollution emission on people over the past 30 years (Antoniou et al. 2019a; Baik et al. 2012a; Ricci et al. 2019d). Factors affecting the airflow and pollutant distribution inside the street canyon include wind direction and speed (Huang et al. 2019c; Zhang et al. 2018e), street canyon structure (Cui et al. 2021b; Reiminger et al. 2020e) (symmetry, asymmetry), building structure (roof (Huang et al. 2009b; Huang et al. 2014b; Llaguno-Munitxa et al. 2017c), balcony (Cui et al. 2020b; Cui et al. 2021b), void deck (Huang et al. 2020c; Huang et al. 2021c)), solar radiation (Lwc et al. 2018a; Mei et al. 2017d), green infrastructure (Huang et al. 2019c; McMullan et al. 2015b), etc. Among these factors, the street canyon structure has a great influence on the airflow and pollutant dispersion inside the canyon (Li et al. 2006). Especially, the void deck can greatly increase the pedestrian-level wind speed inside the canyon (Chen and Mak 2021a; Chew and Norford 2019b). The increase of wind speed on the pedestrian-level can lead to good results that can reduce the damage suffered by pedestrians due to the traffic pollutant dispersion. Void deck is the empty ground floor of public flats, used for social activities and events (such as weddings) by people in tropical countries such as Malaysia and Singapore. Void deck is generally adopted in building design for the ventilation of street canyons and economic purpose (Moosavi et al. 2014c; Muhsin et al. 2017e). However, in the past, void deck received less attention as it was considered undesirable in temperate climates, especially in winter. However, in tropical climates, the outdoor temperature is not low, so that the void deck design is welcomed (Roth and Chow 2012c). The residents living in tropical and subtropical hot and humid regions often experience extreme heat stress in summer since the global warming and the urban heat island effect. One way to relieve this thermal stress and improve thermal comfort is to improve the wind speed inside the street canyons. A field study (Yang et al. 2013b) in Singapore found that the most effective approach to improve thermal

comfort outdoors is to increase wind speed. In Hong Kong, most residents want higher wind speed inside the canyon (Li et al. 2018c). As such, with the emergence of many cities in the tropics, the adoption of street canyons with void deck to enhance pedestrian-level wind speed has become fashionable in recent years (Chen and Mak 2021a; Huang et al. 2020c; Huang et al. 2021c; Weerasuriya et al. 2020f).

Huang et al. (2021c) conducted the two-dimensional numerical simulation in a symmetric street canyon with a street aspect ratio of 1 and analyzed the effects of various street categories and void deck on the pollutant diffusion. The results show that the void deck has a significant effect on the airflow structure and pollutant diffusion inside the canyon, and especially when the void deck at both buildings. Chew and Norford (2018b) studied the effect of changes in the void deck and building height on the pedestrian-level wind environment in a two-dimensional symmetric street canyon. According to their water channel experiments and numerical simulation results, the change in the void deck height has a significantly effect on the pedestrian-level wind speed (up to twice), while the change in the building height has a lesser effect. Also, to enhance the ventilation at the pedestrian level, height of the void deck 4m is sufficient. Continuingly, they extended their study to the three-dimensional street canyon and revealed that when the void deck height is increased from 2 m to 6 m, the pedestrian-level wind speed in the canyon increases from 13% to 59%. However, when the building height increases from 24 m to 48 m, the increase in pedestrian-level wind speed is lower than 10% (Chew and Norford 2019b).

By the above studies, the advantages of the void deck design on the wind environment at the pedestrian-level have been proven. However, the effects of the void deck on the traffic pollutant distribution inside the street canyon have not been clearly identified. Comparisons of the effects of their location, height, and building height on the distribution of traffic pollutant inside 3D street canyons with various void decks have not been reported yet. Also, the effect of void deck on the traffic pollutant distribution at the pedestrians respiration level and both walls is still unknown. Therefore, further studies are still necessary to clarify the effects of void deck on airflow and pollutant dispersion inside the street canyon. More seriously, low wind speed inside the canyon provides favorable conditions for the spread of the influenza, particularly infectious diseases such as the Coronavirus disease 2019 pandemic (Ahmadi et al. 2020a; Pani et al. 2020d; Xu et al. 2020g). The void deck structure is a very promising architectural design that can urgently solve various environmental problems (vehicle exhaust, heat stress, infectious diseases) and provide a comfortable

living environment in the street canyons of the tropical area today.

For the purpose of safeguarding the health of pedestrians and near-road residents, this study provides an insightful understanding of the effects of void deck on the traffic pollutant diffusion inside the street canyons. Fourteen street canyon configurations are chosen to investigate the effects of void deck on airflow and pollutant dispersion under vertical incoming wind. This paper is organized as follows: Fourteen street canyon configurations with and without void deck are given in Section 2.1. Besides, the governing equations for flow and pollutant dispersion, the computational domain, and boundary conditions which is used for CFD simulation are defined in Section 2.2. In addition, the validation study between the numerical results and the WT experimental dataset reported by Kastner-Klein (1999) is performed in Section 2.3 and Section 2.4. The validated CFD models are used to simulate the airflow and traffic pollutant distribution inside the street canyons with and without void deck under the vertical incoming wind. In Section 3, numerical results and discussions are presented. The simulation results are used to evaluate the airflow field and pollutant distribution inside the canyons with the void deck, and to quantitatively assess the effects of the void deck on pedestrians and near-road residents. Especially, to quantify the ventilation capacity of fourteen canyons with the void deck, an evaluation parameter of air exchange rate per hour (ACH) is adopted. Finally, Section 4 draws several conclusions, Section 5 presents limitation and feature work of this paper.

2. Methodology

In this work, based on an 1:150-scaled isolated street canyon model used in WT experiment conducted at University of Karlsruhe University, Germany (Kastner-Klein 1999), 3D street canyons with and without void deck are constructed and validated.

2.1 Street canyon configurations

Fig. 1 shows a sketch of the three-dimensional regular street canyon configuration adopted in this work. As shown in Fig. 1, the regular street canyon is composed of four-lane roads located at the floor of the space between two identical buildings arranged in parallel with each other and two sidewalks on both sides of the canyon. The dimension of each building is set as 1H *(height)*×1H *(width)*×10H *(length)* (where H=0.12 m at the full scale). The length, height and width of the street canyon are the same as that of the building. That is, a wide and long street canyon with H/W=1, L/H=10 is employed as the regular canyon. In Fig. 1a, x, y, and z represent the incoming wind

direction, canyon direction, and sky direction, respectively, in a three-dimensional Cartesian coordinate system with the origin (*x=0*, *y=0*, *z=0*) at the center of the canyon floor. Also, as shown in Fig. 1b, four line sources have the same dimensions are arranged in parallel, and continuously emit sulfur hexafluoride (SF_6) to mimic the exhaust gas emitted by the four-lane roads. To account vehicle exhaust emissions from transverse intersections, four line sources are extended beyond the canyon end by 0.92H on both sides (i.e. the length of each line source is 11.84H, see Fig. 1a) (Salim et al. 2011b). In addition, to clearly clarify the pedestrian exposure risk to pollutants inside the street canyons, the pedestrian respiration height in each case is set to H/12 (1.5 m at the full scale) as in Huang et al. (2019c) (see Fig. 1b). The wind approaches vertically to the 3D street canyon.

With considering the change of the building height (H_b), the height (H_v) and location of void decks, fourteen CFD simulation cases (two cases for regular canyons and twelve cases for the canyons with various void decks) are included in this research. Here, the void deck height is set to H/6 and H/4 (3 m and 4.5 m at the full scale) referring to Chew and Norford (2018b). Based on the regular street canyon configuration, six canyons with various void decks (H_v/W=1/6) are shown in Fig. 2: canyon with void deck at the leeward building (H_b/W=1, Fig. 2a), canyon with void deck at the windward building (H_b/W=1, Fig. 2b), canyon with void deck at both buildings (H_b/W=1, Fig. 2c), canyon with void deck at the leeward building (H_b/W=2, Fig.2d), canyon with void deck at the windward building (H_b/W=2, Fig. 2e), canyon with the void deck at both buildings (H_b/W=2, Fig. 2f). Herein, a building with void deck is modeled as an ideal block with an empty space below (Chew and Norford 2019b).

2.2 CFD model

2.2.1. Governing equations for flow and pollutant dispersion

The airflow inside the street canyon can be considered as incompressible and steady-state turbulent flow. Solar radiation and traffic turbulence are not considered here. Among the common turbulence models, Large Eddy Simulation (LES) often performs better than Reynolds-Meand Navier-Stokes (RANS) model in predicting airflow and pollutant dispersion (Blocken 2015a; Gousseau et al. 2011a; Tominaga and Stathopoulos 2011d). However, LES will require more computational resources and present greater challenges in developing advanced sub-grid scale models and specifying an appropriate time-dependent inlet and wall boundary conditions. Moreover, the steady RANS has unavoidable drawbacks in predicting turbulence, e.g., it does not predict the flow

reattachment length behind building and underestimate the velocity in the wake region. Despite these limitations, RANS models (Allegrini et al. 2014a; Chen 2009a; Cui et al. 2016; He et al. 2017b; Sanchez et al. 2017f) including RSM (Reynolds Stress Model) model (Gromke et al. 2008; Vranckx et al. 2015c) have been well validated and widely used to predict airflow and pollutant dispersion within 2D and 3D urban models.

To assess the dispersion of gaseous pollutants inside the street canyon, the steady-state species transport equation is employed. The equation is following (Huang et al. 2019c):

$$u\frac{\partial C^{\beta}}{\partial x}+v\frac{\partial C^{\beta}}{\partial x}+\omega\frac{\partial C^{\beta}}{\partial x}=\frac{\partial}{\partial x}\left(\left(D_m^{\beta}+\frac{\nu_t}{Sc_t}\right)\frac{\partial C^{\beta}}{\partial x}\right)+\frac{\partial}{\partial y}\left(\left(D_m^{\beta}+\frac{\nu_t}{Sc_t}\right)\frac{\partial C^{\beta}}{\partial y}\right)+\frac{\partial}{\partial z}\left(\left(D_m^{\beta}+\frac{\nu_t}{Sc_t}\right)\frac{\partial C^{\beta}}{\partial z}\right)+S_p \quad (1)$$

In this study, for the simulation on the long street canyon, the isothermal RANS equations with the standard *k-ε* model are adopted (Yim et al. 2010).

2.2.2. Computational domain and grid generation

The computational fluid dynamics (CFD) models are built and meshed with Gambit 2.4.6. The dimension of the CFD domain follow the recommendations in Tominaga et al. (2011d): the inlet is *8H* upstream of the leeward building, while the outlet surface is 19H downstream from the windward building, and the top surface is 8H from the ground, and the both lateral surfaces are placed at 7H from the building side walls, resulting in the domain dimensions of 30H (*length*) × 24H (*width*) × 8H (*height*). Fig. 3 illustrates the CFD domain of the regular canyon without the void deck. The computational domain was meshed using hexahedral grids and all grid cells are perfectly orthogonal without skewness. The total number of grid cells is approximately 4.6 million for each simulation case. The mesh is coarsened above the canyons, upstream of the leeward building, and downstream of the windward building.

The maximum grid increase ratio is limited to 1.08. Inside the canyon and void deck, the grid cells with $\delta x = H/72$, $\delta y = H/12$ and $\delta z = H/72$ are created by using the finer mesh size. Detailed information on the grid sensitivity analysis will be provided in Section 2.3.

2.2.3. Boundary conditions and numerical scheme

All CFD simulations are performed by using the commercial CFD code ANSYS-Fluent 14.5. The boundary conditions are following. At the inlet surface, the atmospheric inlet boundary

conditions (vertical profiles of wind velocity, turbulent kinetic energy and turbulent dissipation rate) are imposed. The inlet profiles of the horizontal wind velocity (U), turbulent kinetic energy (k), and its dissipation rate (ε) are prescribed to match the corresponding experimental conditions, which are given in Eqs. (2)–(4) (Kastner-Klein 1999):

$$\frac{U_z}{U_{ref}} = \left(\frac{z}{z_{ref}}\right)^{0.3} \tag{2}$$

$$k = \frac{u_*^2}{\sqrt{C_u}}\left(1 - \frac{z}{\delta}\right) \tag{3}$$

$$\varepsilon = \frac{u_*^2}{\kappa z}\left(1 - \frac{z}{\delta}\right) \tag{4}$$

The outlet is given as a zero-gradient boundary condition. The top and both sides of the domain have a symmetry boundary condition. The ground and all surfaces of building (leeward wall, windward wall, roof) have a no-slip boundary condition. For the line sources, the volume flow rate of the mixture of air and SF_6 is provided. The SIMPLE pressure-velocity coupling and k-ε turbulence closure is adopted in numerical study. The k-ε turbulence closure have three most commonly used schemes: Standard k-ε, Re-Normalization Group (RNG) k-ε, and Realizable k-ε. Chew and Norford (2018b) and Hang et al. (2012b) reported that the simulation results of the standard k-ε agree better with their experimental results than the RNG k-ε or realizable k-ε simulation results. Therefore, the standard k-ε schemes is used in this study. To the spatial discretization of the governing equations, the second-order upwind scheme is employed. Residuals of simulation are kept at 10^{-6} for all parameters.

2.3 Grid independence analysis

To estimate the mesh independence, three simulation (including the fine, basic and coarse mesh) cases are performed for the regular canyon shown in Fig. 1. For these three simulations, the mesh sizes in the dense area (in-canyon) are H/96, H/72, and H/48, respectively (see Table 1). Therefore, fine, basic and coarse mesh models have 8.2, 4.6 million, and 2.2 million cells, respectively. Fig. 4 plots the demensionless pollutant distribution (K) obtained along three vertical lines (y/H = 0, 1.26, and 3.79, respectively) near both walls of the canyon for the three simulation cases. Herein, the standard k-ε turbulence model with turbulent Schmidt number (Sc_t) of 0.3 is used. For each wall, the vertical lines are 5mm away from that wall. In Fig. 4a, the difference of K between the basic and

coarse grids is large, while the deviation of K becomes very small as increasing the mesh resolution from "basic" to "fine". The K profiles in Fig. 4b depict negligible differences between the three mesh resolutions. Therefore, the basic mesh of 4.6 million cells is determined to be independent grid, and all subsequent simulations are performed with this basic independent grid number.

2.4 Model validation

From the fact that there is no experimental set for 3D long street canyon with the void deck, we carried out a validation study by using the results of a 3D street canyon (model scale 1:150) used for WT experiments performed at the University of Karlsruhe, Germany. Figs. 1 and 3 show the isolated regular canyon configuration with the aspect ratio of 1:1 used in the neutral stratified atmospheric boundary-layer wind tunnel experiment (see the internet database CODASC, https://www.umweltaerodynamik.de/bilder-originale/CODA/CODASC.html). According to their wind-tunnel experiment, the incoming wind was perpendicular to the canyon axis, and two parallel buildings (Hb = Wb = 0.12 m, and L = 1.2 m) were installed on the tunnel floor. A mixture of air and tracer gas (SF_6) with a flow rate of 1000 ppm was continuously emitted from four line sources to mimic the emission of traffic exhaust gas, and the location of the line sources was about 0.23H, 0.35H, 0.65H and 0.77H away from the windward wall, respectively. SF_6 concentrations were measured at specific points on both walls of the canyon and were expressed in dimensionless as follows (Kastner-Klein 1999):

$$K = \frac{CU_{ref}HL}{Q_S} \tag{5}$$

where, K is the dimensionless pollutant concentration, C is the measured volume fraction of SF_6, U_{ref} (= 4.7 m/s) is the free-stream wind velocity at a reference height z_{ref} (= 0.12 m), L (= 1.42 m) is the length of the line source, and Q_s is the source strength. Fig. 5 shows that the CFD simulation results with grid number of 4.6 million and $Sc_t = 0.3$ are in good agreement with the WT experimental data, so the selected parameters can ensure the accuracy of the CFD model. To evaluate quantitatively the current CFD model performance, the statistical validation tests were carried out on the dimensionless pollutant concentrations for the leeward wall, windward wall, and combination of leeward and windward walls based on the CFD-simulated and WT-measured results. Here, the normalized mean square error (*NMSE*), the fractional bias (*FB*), the fraction of predictions within a factor of two of the observations (*FAC2*) and the correlation coefficient (R) are used to evaluate the performance of CFD

models. The model acceptance criteria are as follows (Chang and Hanna 2004; Moonen et al. 2013a): *0.5<FAC2<2*, *-0.3<FB<0.3*, *NMSE<1.5*, *0.7<MG<1.3*, *VG<1.6* and *R>0.8*. From Table 2, it is clear that all statistical indicators are within the acceptable range of model performance.

As shown above, the CFD results are in good agreement with the WT measured data. Thus, the CFD model validated in this study is reliable for simulating airflow and pollutant dispersion inside the street canyons with and without void deck.

3. Results and discussion

Herein, the characteristics of airflow and pollutant distribution were investigated inside the street canyons with the void deck based on the model validation conducted above. The boundary conditions and reference parameters used in each simulation are the identical as that of the model validation.

3.1 Air exchange rate in the street canyon

In this section, we evaluate self-ventilation capability of canyons with and without void deck. ACH which indicates the amount of air exchanged between the street canyon and free atmosphere per unit time, has been widely used as an important indicator to evaluate the ventilation capacity of the canyon (Li et al. 2005a; Liu et al. 2005b; Salim et al. 2011c). For 3D canyons with the void deck, air exchange takes place at both sides and top of street canyons, and at the interface of the canyon and void deck. Therefore, the ACH of the canyon with the void deck can be evaluated as follows by modifying the ACH of the regular canyon (Huang et al. 2019c).

$$\mathrm{ACH}+ = \left(\mathrm{ACH}_{\mathrm{Top}}+\right) + \left(\mathrm{ACH}_{\mathrm{Side1}}+\right) + \left(\mathrm{ACH}_{\mathrm{Side2}}+\right) + \left(\mathrm{ACH}_{\mathrm{Void\ deck1}}+\right) + \left(\mathrm{ACH}_{\mathrm{Void\ deck2}}+\right) \quad (6)$$

$$\mathrm{ACH}- = \left(\mathrm{ACH}_{\mathrm{Top}}-\right) + \left(\mathrm{ACH}_{\mathrm{Side1}}-\right) + \left(\mathrm{ACH}_{\mathrm{Side2}}-\right) + \left(\mathrm{ACH}_{\mathrm{Void\ deck1}}-\right) + \left(\mathrm{ACH}_{\mathrm{Void\ deck2}}-\right) \quad (7)$$

where $\mathrm{ACH}_{\mathrm{Top}}$, $\mathrm{ACH}_{\mathrm{Side1}}$, $\mathrm{ACH}_{\mathrm{Side2}}$, $\mathrm{ACH}_{\mathrm{void\ deck1}}$, $\mathrm{ACH}_{\mathrm{void\ deck2}}$ are the values of ACH at each plane where air exchange occurs, respectively. The positive ACH (ACH+) means air exiting from the canyon, while negative ACH (ACH-) means air entering into the canyon. The ACH at an air exchange plane consists of the mean ($\overline{\mathrm{ACH}}$) and turbulence (ACH′) components:

$$\mathrm{ACH} = \overline{\mathrm{ACH}} + \mathrm{ACH}' \quad (8)$$

where $\overline{\mathrm{ACH}}$, ACH′ are induced by exchange by the mean velocity and the velocity fluctuation respectively. The ACH′ at each air exchange plane can be written as (Li et al. 2005a).

$$\mathrm{ACH}'_{\mathrm{Top}+} = -\mathrm{ACH}'_{\mathrm{Top}-} = \frac{1}{\sqrt{6}} \int_{\Gamma_1} \sqrt{k} d\Gamma_1 \tag{9}$$

$$\mathrm{ACH}'_{\mathrm{Side1}+} = -\mathrm{ACH}'_{\mathrm{Side1}-} = \frac{1}{\sqrt{6}} \int_{\Gamma_2} \sqrt{k} d\Gamma_2 \tag{10}$$

$$\mathrm{ACH}'_{\mathrm{Side2}+} = -\mathrm{ACH}'_{\mathrm{Side2}-} = \frac{1}{\sqrt{6}} \int_{\Gamma_3} \sqrt{k} d\Gamma_3 \tag{11}$$

$$\mathrm{ACH}'_{\mathrm{Void\ deck1}+} = -\mathrm{ACH}'_{\mathrm{Void\ deck1}-} = \frac{1}{\sqrt{6}} \int_{\Gamma_4} \sqrt{k} d\Gamma_4 \tag{12}$$

$$\mathrm{ACH}'_{\mathrm{Void\ deck2}+} = -\mathrm{ACH}'_{\mathrm{Void\ deck2}-} = \frac{1}{\sqrt{6}} \int_{\Gamma_5} \sqrt{k} d\Gamma_5 \tag{13}$$

Where $\Gamma_1=L\times W$, $\Gamma_2=H\times W$, $\Gamma_3=H\times W$, $\Gamma_4=H_{vd}\times L$, $\Gamma_5=H_{vd}\times L$ are the areas of the corresponding air exchange planes. Table 3 and 4 tabulate the positive and negative dimensionless air exchange rate (ACH+) for the fourteen street canyons with and without void deck. According to the analysis of the air exchange rate of the two regular canyons (H_b/W=1 or 2), the values are 0.16 and 0.11, respectively, which are the minimum values compared to the canyons with the void deck. This means that the void deck has a very positive effect on the ventilation of the canyon by enhancing the airflow and the pollutant diffusion to the outside of the canyon. Also, for the two regular canyons, ACH' values are 77.3% and 75.5%, respectively, which are higher than that of the canyons with the void deck. This finding proves that the void deck significantly reduces disturbances inside the canyon. The detailed analyses on the effects of void deck on the ACH of the canyon are as follows.

Firstly, it can find that the void deck greatly improves the ventilation capacity of the canyon. The street canyons with void deck have higher ACH values than regular canyons without the void deck. Regardless of the height of the building and the void deck, the ACH of the canyons has the maximum values when the void deck is at both buildings, followed by the canyons with the void deck at the leeward building. For the canyons with the void deck at the windward building, the ACH values are the smallest. This is obviously related to the basic airflow inflowing to the canyon through the void deck. For example, for the canyon (H_b/W=1) with void deck (H_v/W=1/6), when the void deck is at both buildings, the pollutants generated from the canyon floor are removed directly out of the canyon by the strong basic airflow flowing through the void decks located at the bottom of two buildings, so the ACH value is the largest as 0.29. Also, comparing the ACH values of the street canyons where the void deck is at the leeward building or the windward building, the air exchange

rate of the canyon where the void deck is at the leeward building (0.27) is higher than for the canyon (0.18) with the void deck at the windward building since the strength of the basic airflow passing through the canyon is clearly stronger when the void deck is at the leeward building. Specifically, for the canyons with the void deck at the leeward building ($H_b/W=1$), the $\overline{ACH}$ values are zero at both sides of the canyon. This means that for the canyons with the void deck at the leeward building, there are no airflow components inflowing from both sides of the canyon. The these features of three basic airflows have the opposite effect on the perturbation change of the turbulence. In other words, the ACH' value of the canyon with the smallest basic airflow strength(when the void deck is located at the windward building) is the largest, followed by the canyon where the void deck is located at the leeward building. Among the twelve canyons with void deck, the canyons ($H_b/W=1$) with void deck ($H_v/W=1/4$) at both buildings have the highest air exchange rate (0.38). When the void deck ($H_v/W=1/6$) is at the windward building ($H_b/W=2$), the ACH value is the smallest (0.12).

Secondly, the increase of the void deck height results in the increase of the ventilation capacity of the canyon. As the void deck height increases, the velocity of the basic airflow inflowing to the canyon through the void deck increases, and this strengthened airflow removes more pollutants out of the canyon, thus increasing the canyon's ACH value. Conversely, the perturbation change of the turbulence inside the canyon is suppressed that much, and the ACH' value is reduced.

Thirdly, the ventilation capacity of the street canyons with the void deck reduces as the building height increases. For the regular canyons without the void deck, the ACH value (0.11) of the regular canyon ($H_b/W=2$) is lower than that (0.16) of the regular canyon ($H_b/W=1$). This is because the higher the building height, the less free-stream through the canyon top can affect the bottom of the canyon where the pollutants are generated. For the canyons with the void deck, the higher the building height, the stronger the airflow inflowing to the canyon through the void deck, so more pollutants are removed out of the canyon. However, as the building height increases, the canyon volume increases, resulting in a smaller ACH.

From the above analysis, it can find that the air exchange rate of the canyon is large with the lower building height and higher the void deck height. In particular, the ACH of the canyon with the void deck at both buildings has the highest value.

3.2 Airflow and pollutant distributions on the vertical central plane

In this section, the effects of change in the different location (when the void deck is at the leeward

building, windward building or both buildings) and height (H_v/W=1/6 or 1/4) of the void deck on the airflow and pollutant distributions of the vertical central plane inside the canyons (H_b/W=1 or 2) are investigated. Fig. 6 depicts the airflow patterns and dimensionless pollutant distributions on the vertical central plane of the regular canyons without the void deck. For the regular canyon (H_b/W=1) (see Fig. 6a), a large clockwise vortex is formed inside the canyon. This vortex is generated by free-stream passing above the canyon. The core of this vortex is slightly upward and to the right from the center of the canyon, and the airflow speed at the core of the vortex is weaker than at the building walls or the ground. The velocity of the downflow on the windward wall is faster than the level flow near the ground or the upflow on the leeward wall. Due to this large vortex, many pollutants are accumulated on the leeward side of the canyon, and the pollutant concentration therein is much higher than that of the windward side. Also, a small clockwise vortex is obtained above the roof of the leeward building, and two small counterclockwise vortices are formed at both corners inside the canyon. The small vortex above the roof of the leeward building is caused by the severe separation when the free-stream collides at the upleft edge of the leeward building, and is found in all canyons discussed in this paper (see Figs. 7 and 8). The small vortices on both corners of the in-canyon are formed by the action between the canyon walls and the large vortex. Contrary to the expectation, for the regular canyon (H_b/W=2) (see Fig. 6b), there is no large vortex inside the canyon. For this case, the airflow streams start at a point (about H/5 above the ground) near the leeward wall and spread out into the canyon, the velocity of the airflow is low near the ground and windward wall, and it is slightly large at the upper half of the leeward wall. Thus, a small vortex with a core slightly lower than the building height and slightly biased toward the windward building is formed inside the canyon. Due to this small vortex, the pollutant concentration near the upper part of the windward wall is low, and the pollutant concentration at the rest part is very high. In particular, pollutants accumulate more on the windward wall by the airflow moving towards the windward side near the bottom of the canyon. Figs. 7 and 8 depict the airflow and dimensionless pollutant distribution patterns on the vertical central plane inside the street canyons with the void deck. From Figs. 6, 7, and 8, three features are observed.

First, it can note that the void deck greatly changes the airflow field and pollutant distribution inside the canyon. As shown in Figs. 7 and 8, airflow and pollutant distribution patterns on the vertical central plane inside the canyons with void deck are quite different from that of the regular canyons. For example, for the canyon (H_b/W=1) with void deck at the leeward building (see Figs. 7a and b),

the strong airflow inflowing through the void deck of the leeward building moves toward the windward side, and flows upward along the windward wall, and finally merges with the free-stream above the roof of the windward building. By this strong airflow, pollutants are removed out of the canyon and only slightly accumulate on the windward wall. Also, the large vortex of the regular canyon (see Fig. 6a) is completely disrupted inside the canyon, instead two smaller counter-clockwise vortices are formed and two small vortices are generated at the corner and above the roof of the windward building. For the canyon with void deck at the windward building (see Figs. 7c and d), the airflow inflowing through the void deck of the windward building (the velocity of the airflow is lower than the airflow inflowing through the void deck of the leeward building in Figs. 7a and b.) moves toward the leeward side, and flows upward along the leeward wall, and finally merges with the free-stream. Therefore, the smaller clockwise and right-biased vortex is formed inside the canyon (see Fig. 6a), and a small vortex is observed at the left corner inside the canyon. The pollutants accumulate near the leeward wall inside the canyon by this strong airflow, and the degree is smaller than the case of the regular canyon (Fig. 6a). For the canyon with void deck at both buildings (see Figs. 7e and f), most of the strong airflow that inflowing through the void deck of the leeward building passes the bottom of the street canyon and the void deck of the windward building in turn, and a small fraction flows upward along the windward wall. Therefore, pollutants can not flow upward along the windward wall, but travel to the void deck of the windward building, where it is eventually removed out of the canyon. At that time, the pollutant concentration on the vertical central plane is the lowest. Inside the street canyon (upper the void deck height), two counter-clockwise vortices are formed. The airflow and pollutant distribution inside the canyons ($H_b/W=2$) with void deck is similar to that of the canyons ($H_b/W=1$) with void deck (see Fig. 8).

Second, as the void deck height increases, the pollutant concentration on the vertical central plane inside the canyons decreases. For the canyons ($H_b/W=1$) with the void deck, comparing Figs. 7a and b, Figs. 7c and d, Figs. 7e and f, it can be seen that even if the height of the void deck is increased from H/6 to H/4, the airflow field and pollutant pattern inside the canyon do not change significantly. However, the velocity and width of the basic airflow is increased, and the strength of the main vortex inside the canyon is weakened. Since the pollutants generated at the bottom of the street canyons are affected by these basic airflow, the pollutant distribution inside the canyon shows a tendency to slightly decrease as the height of the void deck increases. These features are the same ones even when the height of the building is *2H* (see Figs. 8a and b, Figs. 8c and d, Figs. 8e and f).

The reason is that as the height of the void deck increases, the strength of the airflow flowing into the canyon through the void deck increases, and as a result, the strength of the basic flow inside the canyon becomes stronger. For example, comparing Figs. 8a and b, it can be noted that there is a basic airflow with a width almost equal to the height of the void deck inside the canyon, and the width of the basic airflow increases as the height of the void deck increases. As the width of the basic airflow increases, the main vortices are compressed that much, and as a result, the vortex strength becomes weaker. In particular, for the canyons with void decks at both sides (see Figs. 7e and f, Figs. 8e and f), the basic airflow strength is the strongest because the airflow passes directly through the canyon. Therefore, for these cases, a relatively large change of airflow speed is observed according to the increase the void deck height, and the pollutant distribution is also observed very faintly.

Third, the building height increases have a positive effect on reducing the pollutant concentration of the vertical central plane. Comparing Figs. 7a and 8a, Figs. 7b and 8b, as the height of the building increases, among the two vortices existing inside the canyon, the vortex at the lower part is greatly developed in the direction of the building height, while the vortex at the upper part is greatly weakened. The reason is that the higher the building, the more the vortex at the lower part expands in the direction of the building height due to the basic airflow flowing upward along the windward wall. As this process deepens, the upper vortex becomes smaller by the free-stream passing through the canyon top and the vortex that develops below it. Also, the intensity of the basic airflow passing through the void deck and the canyon becomes much stronger. Therefore, as the height of the building increases, the pollutant distribution of inside the canyon is greatly reduced. The same is true for the canyon with void deck at the windward building (see Figs. 7c and 8c, Figs. 7d and 8d). For these cases, the concentration of pollutants inside the canyon is reduced more than other cases. For the canyons with the void deck at both buildings (see Figs. 7e and 8e, Figs. 7f and 8f), the vortex at the lower part is enlarged and the vortex at the upper part disappears due to the height of the building increases. As shown in Fig. 8e, the strength of the vortex inside the canyon is weak because a small share of the airflow inflowing into the void deck of the leeward building flows upward through the windward wall, and only a small share of it contributes to the formation of the vortex. Therefore, unlike Fig. 7e, a small vortex cannot be formed in the space between the free-stream passing through the canyon top and the vortex inside the canyon. In particular, for these cases, the strength of the basic airflow is the strongest since there are no obstacles to obstruct the airflow. By these basic airflows, traffic pollutants emitted from the canyon floor are almost completely removed from the canyon.

In summary, it can note that for the canyons with the void deck, the traffic pollutant diffusion is suppressed by the basic airflow that inflows from the void deck and passes through the pollutant generating region, and as a result, the void deck provides the advantageous environment for removing pollutants inside the canyon.

3.3 Airflow and pollutant distributions at the pedestrian respiration level

Fig. 9 shows the airflow and pollutant distribution patterns at the pedestrian respiration level (1.5 m at the full scale) in the regular canyons without the void deck. For the regular canyon ($H_b/W=1$) (Fig. 9a), outside the street canyon, two small vortices are formed on both sides of the leeward building and at the back of the windward building, respectively. Meanwhile, inside the canyon, the airflow that entered near the windward wall on both side of the canyon flows toward the center of the leeward wall. Therefore, the pollutant concentration is low near both sides and near the windward wall of the canyon, and high in the central part of the canyon and near the leeward wall. For the regular canyon with the building ($H_b/W=2$) (Fig. 9b), the small vortices mentioned above (existing for Fig. 9a case) are further developed larger outside the canyon. Inside the canyon, the airflow generated at two points near the windward wall on both sides of the canyon moves toward the center of the canyon and collides with each other, forming two symmetrical small vortices near the windward wall of the center of the canyon. Due to these airflow features, the pollutant concentration is low on both sides of the canyon, but a relatively wide high-pollutant region is formed in the center of the canyon. That is, when the height of the building increases, the pollutant concentration of the respiration plane near the windward wall becomes much higher. Figs. 10 and 11 show the airflow and pollutant distribution patterns at the pedestrian respiration height for the canyons ($H_b/W=1$ or 2) with void deck ($H_v/W=H/6$ and $H/4$). From Figs. 9-11, it can be seen that for the canyons with and without void deck, the airflow structures and pollutant distribution patterns at the pedestrian respiration height are symmetrical about the vertical central line of the canyon. In addition, for a quantitative comparison, the mean pollutant concentration (K) values at the pedestrian respiration planes near both walls of fourteen canyons are given in Fig. 12. From the comparison analysis of Figs. 9-12, the effects of building height and the height and location of the void deck on the airflow and pollutant dispersion at the pedestrian respiration height are analyzed as follows.

First, the void deck has a significantly effect on reducing the pollutant concentration at the pedestrian respiration planes inside the canyon. Comparing Fig. 9 with Figs. 10 and 11, it is find that

for the canyons with the void deck, the pollutant concentration patterns at the pedestrian respiration height have completely new shapes, which is different to that in the regular canyons without the void deck. For example, for the canyon (H_b/W=1) with the void deck (H_v/W=1/6), when the void deck is at the leeward building (Fig. 10a), the pollutant pattern near the leeward wall is not observed. However, near the windward wall, the pollutants are distributed parallel with almost the same width along the windward wall. This is explained by the fact that unlike in the regular canyon (H_b/W=1), the basic airflow passing through the void deck of the leeward building moves the pollutants generated from the line sources toward to the windward wall at almost the same speed in parallel. Therefore, for this case, many pollutants are accumulated on the respiration plane near the windward wall. In Fig. 12, comparing with the case of the regular canyon (K_A=40.4, K_B=10.6), the mean K at the respiration plane near the leeward building is zero (K_A=0) and that at the respiration plane near the windward building is much higher (K_B=24.0). When the void deck is at the windward building (Fig. 10c), the airflow that collided with the windward wall of the leeward building and splits in two directions is reversed as it passes both sides of the leeward building, resulting in the some of the airflow enters through the void deck of the windward building, some airflow enters to the canyon directly through both sides of the canyon. These airflows reach the leeward wall and then creat two small vortices symmetrical about the vertical central line of the canyon near the leeward wall. As a result, many pollutants accumulate at the respiration plane (K_A=42.3), and tiny at the respiration plane (K_B=2.8). The pollutant distribution near the leeward wall is almost parallel to the leeward wall in the central part and slightly protrudes where two small vortices exist. Also, the pollutant concentration in the two small vortex regions is slightly higher than that in the middle region, and is the lowest on both sides of the canyon. When the void deck is at both buildings (Fig. 10e), due to the bottom of the canyon is opened by the two void decks, the strong airflow passes through the canyon unaffected by any obstacle, meanwhile the pollutants are removed out of the canyon by this airflow. Therefore, the pollutant distribution on the pedestrian respiration planes near the leeward and windward building is hardly observed or significantly low (K_A=0, K_B=8.4).

Second, the increase of the void deck height has a distinct effect on the pollutant distribution at the pedestrian respiration height of the canyon. When the void deck is at the leeward building (H_b/W=1) (Fig. 10a and b), observing the airflow distribution at the respiration height, the velocity of the basic airflow passing through the void deck of the leeward building slightly increases as the void deck height increases. Therefore, when void deck height is H/4, more pollutants are removed

out of the canyon by the stronger basic airflow (Fig. 7b) that inflows through the void deck and passes the canyon floor and flows upward along the windward wall. As a result, less pollutant distribution (K_A=0, K_B=19.5) is observed at the respiration plane than when the void deck height is H/6. When the void deck is at the windward building (H_b/W=1) (Fig. 10c and d), the increase of the void deck height leads to the increase of the airflow streamline density inflowing through the void deck of the windward building (the airflow streamline density indicates the strength of airflow). Due to this strengthened airflow, when the void deck height is H/4, the mean pollutant concentration (K_A=37.7) of the respiration plane near the leeward wall is slightly decreased compared to that with the void deck height H/6, and that (K_B=3.3) of the respiration plane near the windward wall is slightly increases. When the void deck is at both buildings (H_b/W=1) (Fig. 10e and f), the velocity of the basic airflow passing through the canyon floor increases significantly as the void deck height increases, and by this airflow, pollutants are almost completely removed out of the canyon. Therefore, in Fig. 10e there are two small and low pollutant concentration distribution patterns at both ends of the leeward building, and in Fig. 10f no pollutant distribution pattern is observed at all (K_A=0, K_B=6.6). Also, as shown in Fig. 11, for the canyons (H_b/W=2) with the void deck, as the void deck height increases, the velocity of the airflow flowing into the canyon through the void deck slightly increases. Because of this, as in the case of the canyons (H_b/W=1) with the void deck (Fig. 10), the pollutant concentrations at the respiration planes are reduced. However, the pollutant pattern change is quite small. To be concrete, according to the quantitative analysis of the mean K at the pedestrian respiration planes (Fig. 12), when the void deck is at the leeward building (Figs. 11a and b), the mean pollutant concentration (K_B=13.9) is slightly reduced compared to the case that the void deck height is H/6 (K_B=18). When the void deck is at the windward building (Figs. 11c and d), the mean K at the respiration plane near the leeward wall decreases from 36.4 to 31.1. When the void deck is at both buildings (Figs. 11e and f), the mean K at the respiration plane near the windward wall decreases from 7.5 to 6.9. This means that when the building height is higher, the variation of the void deck height has minor effect on the mean pollutant concentration.

Third, from the comparison between Figs. 10 and 11, it can be seen that for the canyons with the void deck, the higher the building height, the lower the pollutant concentration at the respiration level, unlike in the regular canyon. This is because the velocity of the basic airflow flowing into the canyon through the void deck increases significantly as the building height increases. For example, when the void deck (H_v/W=1/4) is at the leeward building, comparing Figs. 10b and 11b, for the canyon with

building height 2H, lower pollutant distribution pattern is observed at the respiration level due to the velocity of the airflow inflowing through the void deck of the leeward building is much faster than that for the canyon with building height H. For this case, the mean *K* of the respiration plane near the windward wall decreases from 19.5 to 13.9 as the building height increases. When the void deck (H_v /W=1/4) is at the windward building (Figs. 10d and 11d), as the building height increases, the velocity of the airflow inflowing through the void deck of the windward building increases, and eventually the pollutants are more compressed toward to the leeward wall. For this case, the mean *K* of the respiration plane near the leeward wall reduces from 37.7 to 31.1, and the mean *K* of the respiration plane near the windward wall decreases from 3.3 to almost 0. When the void deck (H_v/W=1/4) is at both buildings (Figs. 10f and 11f), there are no pollutant patterns in the street canyon due to the pollutants are removed out of the canyon through the void deck of the windward building by the basic airflow passing through the void decks on both sides of the canyon. From Fig. 12, when the building height is H or 2H, the mean *K* of the respiration planes near the windward wall is very low as 6.6 and 6.9, respectively.

From the above analysis, it can find that increasing the height of the void deck and building can significantly lower the pollutant concentration at the pedestrian respiration height of the street canyon, can provide a very good environment for pedestrian health.

3.4 Pollutant distributions on the canyon walls

The pollutant concentration distribution on both walls of the canyon is closely related to the health of indoor residents. Therefore, in this section, we evaluate the pollutant concentration levels on both walls of the canyon with the void deck. Fig. 13 depicts the pollutant distribution on both walls of the regular canyons (H_b/W=1 or 2) without the void deck. For the regular canyon (H_b/W=1) (Fig. 13a), the pollutant pattern on both walls likes a “saddle” shape, and symmetrical distributions along the vertical central line, and the pollutant concentration of the central part is higher than that of the sides. The pollutant concentration of the leeward wall is much higher than that of the windward wall. This is because fresh airflow inflowing from both sides of the canyon flows toward the leeward wall by the large vortex (see Fig. 9a and 6a) formed in the center part of the canyon and moves pollutants to the center of the leeward wall. For the regular canyon (H_b/W=2) (Fig. 13b), pollutant patterns on both walls have symmetrical distribution in the shape of a “mushroom cap”. The pollutant concentration in the middle part of the leeward wall is slightly higher than that of the regular canyon

(H_b/W=1). However, many pollutants are accumulated on the windward wall by the airflow (see Fig. 9b and 6b) flowing from the leeward wall to the windward wall inside the canyon, so the high-pollutant region is formed in the middle part of the windward wall. Figs. 14 and 15 show the pollutant distribution patterns on both walls for the street canyons with the void deck, with building height of H and 2H, respectively. In Fig. 16, the mean dimensionless *K* values on both sides of the street canyons with and without void deck are quantitatively compared. From Figs. 13-16, comparing the pollutant distribution on both walls of canyons with and without void deck, we can find several features.

First, mean *K* on the wall of the buildings with the void deck inside the canyon is very low, almost equal to zero. At walls with void deck in Figs. 14 and 15, the pollutant distribution patterns are not observed. The reason is that the pollutants generated from the canyon floor are directly removed out of the canyon by the basic airflow, as shown in Figs. 7 and 8. However, various pollutant distribution patterns appear on the walls without the void deck. For example, for the canyons with the void deck at the leeward building, the pollutant contour lines are distributed almost horizontally along the canyon (see Figs. 14a and b, Figs. 15a and b). This is because the airflow inflowing through the void deck of the leeward building moves the pollutants to the windward wall with almost the same strength (see Figs. 10a and b, Figs. 11a and b). In particular, for these cases, unlike regular canyons without void deck (Fig. 9), since there is no airflow inflowing from both sides of the canyon (see Table 4, for the canyons with the void deck at the leeward wall, $\overline{\mathrm{ACH}}_{Side1}$ and $\overline{\mathrm{ACH}}_{Side2}$ are almost zero), the pollutants do not collect in the middle of the canyon and are evenly distributed horizontally on the windward wall. For the canyons with the void deck at the windward building, pollutant patterns on the leeward wall resemble a “horn” and form a symmetrical distribution (see Figs. 14c and d, Figs. 15c and d). While the basic airflow inflowing through the void deck of the windward building reaches the leeward wall and then flows toward both sides of the canyon, it loses kinetic energy as a result of the action with the other airflow inflowing from both sides of the canyon (see Figs. 10c and d, Figs. 11c and d). Therefore, the airflow velocity is reduced in this active region, pollutants are accumulated, and finally pollutant distribution patterns similar to “horn” are formed on the leeward wall. For the canyons with the void deck at on both buildings, pollutants are removed out of the canyon by the strong basic airflow passing through the bottom of the canyon (see Figs. 7e and f, Figs. 8e and f), so the pollutant distribution is not observed on both walls (Figs. 14e and f, Figs. 15e and f).

Second, increasing the void deck height reduces the pollutant concentration of the canyon walls.

For the canyons with the void deck, from the comparison of Figs. 14 and 15, it can be seen that the pollutant concentration on the walls without the void deck decreases when the void deck increases from H/6 to H/4. This is because as the void deck height increases, the velocity of the basic airflow passing through the void deck the canyon is increased (see Figs. 7 and 8). As a result, more pollutants are moved out of the canyon by these strong airflow. Especially, for the canyons with the void deck at both buildings, the pollutant distribution patterns on the canyon walls are not observed (Figs. 14e and f, Figs. 15e and f). This shows that for the canyons with the void deck at both buildings, void deck height of H/6 (3 m at a full scale) is sufficient to remove pollutants on both walls.

Third, for the canyons with the void deck, the pollutant concentration on both walls of the canyon decreases as the building height increases. For the regular canyons, it can be seen that as the building height increases, the mean K on the leeward wall reduces from 26.0 to 18.3 and the mean K on the windward wall increases from 6.9 to 22.0 (see Fig. 16). However, for the canyons with the void deck, the mean K on both walls reduces when the building height increases from H to 2H. From Fig. 14 and 15, for the canyons with void deck of the same height and location, the strength of the basic airflow passing through the void deck is much stronger for the canyons ($H_b/W=2$) than for the canyons ($H_b/W=1$). The stronger the airflow, the more pollutants are released out of the canyon.

From this, we can find that for the canyons with the void deck, the higher the void deck and the building height, the lower the pollutant concentration on both walls of the canyon. Especially when the void deck is at both buildings, the mean concentration on the canyon walls is extremely low , so it could provide a very good living environment for the near-road residents compared to the regular canyon.

4. Conclusions

In this paper, we explored the effects of void deck on the airflow and pollutant diffusion characteristics inside the street canyon. In 3D street canyon numerical simulation validated by WT data, different building heights, various locations and heights of the void deck are considered. From the analysis of the CFD numerical simulation results, the following conclusions are reported.

The void deck location has a significantly effect on the airflow and pollutant distribution inside the street canyon. Unlike the regular canyons, for the canyons with the void deck, pollutants are removed out of the canyon by the strong fresh airflow inflowing to the canyon through the void deck. Therefore, for the canyons with the void deck, the ACH is significantly increased and ACH′ (the

perturbation change of turbulence) is reduced compared to the regular canyons. When the void deck is at both buildings, the strong airflow passes directly through the bottom of the canyon, so the ACH is the highest, followed by the case where the void deck is at the leeward building. When the void deck is at the windward building, due to the reverse airflow inflows to the canyon through the void deck of the windward building, the strength of airflow is the weakest and as a result the ACH is the smallest.

As the void deck height increases, the strength of airflow inflowing to the canyon through the void deck becomes stronger. This airflow characteristic allows more pollutants to be removed out of the canyons for the canyons with higher void deck height. Therefore, ACH increases as the void deck height increases. In particular, the effect of void deck height is the greatest when the void deck is located at both buildings, and is the smallest when the void deck is located at the windward building. In addition, the pollutant concentration at both walls of the canyon and at the pedestrian respiration height also decreases as the void deck height increases. Since pollutants are moved by the strong airflow flowing into the canyon through the void deck, the mean pollutant concentration on the wall of the building with the void deck and on the pedestrian respiration plane close to it is near zero. The mean pollutant concentration on the wall of the building without the void deck and on the pedestrian respiration plane close to it is lower than that of the regular canyon except for one case (for the canyon (H_b/W=1) with the void deck at the leeward building). That is, as the void deck height increases, a very good environment for the health of pedestrians and near-road residents inside the street canyon can be provided. For the canyon with the void deck at both buildings, void deck height of H/6 (3 m at a full scale) is sufficient.

For the canyons with the void deck, building height has a significantly influence on the intensification of pollutant diffusion inside the canyon. For the canyons with the void deck, when the building height increases, the strength of airflow inflowing to the canyon through the void deck increases, and more pollutants are removed out of the canyon. However, at this time, the ACH decreases. This reason is that the canyon volume increases as the building height increases. In addition, the pollution concentration at both walls of the canyon and at the pedestrian respiration height also decreases with increasing building height, which has the same tendency as when the void deck height increases. However, the increase in the building height has a more pronounced effect than the increase in the void deck height. That is, the void deck is very advantageous in reducing the risks of pollutant of the pedestrians and residents inside the street canyons composed of high-rise buildings.

From the above conclusions, we can find that the void deck is a very effective architectural feature for improving traffic pollution in urban canyons in the tropics. In the future, the void deck can be used very effectively to reduce the damage to pedestrians and residents caused by traffic pollutants in a street canyon consisting of high-rise buildings.

Acknowledgements

This work was supported by the Scientific and Innovative Action Plan of Shanghai (No.20dz1204000) and the National Natural Science Foundation of China (Grant No. 52106102 and 51536006).

Declarations

- Ethics approval and consent to participate

  Not applicable

- Consent for publication

  Not applicable

- Authors Contributions

Chung Hyok Sin is the lead author of this paper, and has contributed to establish and calculate the numerical models and drafted this paper.

Yang Luo has mainly contributed to guide the establishment of numerical models and the paper revision.

Kwang Song Jon has contributed to the processing of the numerical results and drawn the figures and tables.

Peng-Yi Cui has contributed to the processing of the numerical results and drawn the figures and tables.

Yuan-dong Huang as the corresponding author and supervision, has carefully edited the grammar, spelling, sentence structures of this paper.

All authors read and approved the final manuscript.

- Funding

This work is supported by the Scientific and Innovative Action Plan of Shanghai (No.20dz1204000) (the establishment and calculation of numerical models) and National Natural Science Foundation of China (Grant No. 52106102 and 51536006) (analysis and interpretation of data, as well as manuscript polishing).

- Competing interests

The authors declare that they have no competing interests

- Availability of data and materials

The datasets used and/or analysed during the current study are available from the corresponding author on reasonable request.

References

Ahmadi M, Sharifi A, Dorosti S, Jafarzadeh Ghoushchi S, Ghanbari N (2020a) Investigation of effective climatology parameters on COVID-19 outbreak in Iran. Sci Total Environ 729:138705. https://doi.org/10.1016/j.scitotenv.2020.138705

Allegrini J, Dorer V, Carmeliet J (2014a) Buoyant flows in street canyons: Validation of CFD simulations with wind tunnel measurements. Build Environ 72:63-74. https://doi.org/10.1016/j.buildenv.2013.10.021

Antoniou N, Montazeri H, Neophytou M, Blocken B (2019a) CFD simulation of urban microclimate: Validation using high-resolution field measurements. Sci Total Environ 695:133743. https://doi.org/10.1016/j.scitotenv.2019.133743

Baik J-J, Kwak K-H, Park S-B, Ryu Y-H (2012a) Effects of building roof greening on air quality in street canyons. Atmos Environ 61:48-55. https://doi.org/10.1016/j.atmosenv.2012.06.076

Blocken B (2015a) Computational Fluid Dynamics for urban physics: Importance, scales, possibilities, limitations and ten tips and tricks towards accurate and reliable simulations. Build Environ 91:219-245. https://doi.org/10.1016/j.buildenv.2015.02.015

Chang JC, Hanna SR (2004) Air quality model performance evaluation. Meteorol Atmos Phys 87https://doi.org/10.1007/s00703-003-0070-7

Chen K, Norford L (2017a) Evaluating Urban Forms for Comparison Studies in the Massing Design Stage. Sustainability 9:987. https://doi.org/10.3390/su9060987

Chen L, Mak CM (2021a) Numerical evaluation of pedestrian-level wind comfort around “lift-up” buildings with various unconventional configurations. Build Environ 188:107429. https://doi.org/10.1016/j.buildenv.2020.107429

Chen Q (2009a) Ventilation performance prediction for buildings: A method overview and recent applications. Build Environ 44:848-858. https://doi.org/10.1016/j.buildenv.2008.05.025

Chew LW, Glicksman LR, Norford LK (2018a) Buoyant flows in street canyons: Comparison of RANS and LES at reduced and full scales. Build Environ 146:77-87. https://doi.org/10.1016/j.buildenv.2018.09.026

Chew LW, Norford LK (2018b) Pedestrian-level wind speed enhancement in urban street canyons with void decks. Build Environ 146:64-76. https://doi.org/10.1016/j.buildenv.2018.09.039

Chew LW, Norford LK (2019b) Pedestrian-level wind speed enhancement with void decks in three-dimensional urban street canyons. Build Environ 155:399-407. https://doi.org/10.1016/j.buildenv.2019.03.058

Cui D, Li X, Du Y, Mak CM, Kwok K (2020b) Effects of envelope features on wind flow and pollutant exposure in street canyons. Build Environ 176:106862. https://doi.org/10.1016/j.buildenv.2020.106862

Cui D, Li X, Liu J, Yuan L, Mak CM, Fan Y, Kwok K (2021b) Effects of building layouts and envelope features on wind flow and pollutant exposure in height-asymmetric street canyons. Build Environ 205:108177. https://doi.org/10.1016/j.buildenv.2021.108177

Cui P-Y, Li Z, Tao W-Q (2016) Buoyancy flows and pollutant dispersion through different scale urban areas: CFD simulations and wind-tunnel measurements. Build Environ 104:76-91. https://doi.org/10.1016/j.buildenv.2016.04.028

Gousseau P, Blocken B, Stathopoulos T, van Heijst GJF (2011a) CFD simulation of near-field pollutant dispersion on a high-resolution grid: A case study by LES and RANS for a building group in downtown Montreal. Atmos Environ 45:428-438. https://doi.org/10.1016/j.atmosenv.2010.09.065

Gromke C, Buccolieri R, Di Sabatino S, Ruck B (2008) Dispersion study in a street canyon with tree planting by means of wind tunnel and numerical investigations – Evaluation of CFD data with experimental data. Atmos Environ 42:8640-8650. https://doi.org/10.1016/j.atmosenv.2008.08.019

715 Hang J, Li Y, Sandberg M, Buccolieri R, Di Sabatino S (2012b) The influence of building height variability on pollutant dispersion and pedestrian
716 ventilation in idealized high-rise urban areas. Build Environ 56:346-360. https://doi.org/10.1016/j.buildenv.2012.03.023
717 He L, Hang J, Wang X, Lin B, Li X, Lan G (2017b) Numerical investigations of flow and passive pollutant exposure in high-rise deep street canyons
718 with various street aspect ratios and viaduct settings. Sci Total Environ 584-585:189-206. https://doi.org/10.1016/j.scitotenv.2017.01.138
719 Huang T, Niu J, Xie Y, Li J, Mak CM (2020c) Assessment of "lift-up" design's impact on thermal perceptions in the transition process from indoor to
720 outdoor. Sustainable Cities and Society 56:102081. https://doi.org/10.1016/j.scs.2020.102081
721 Huang Y-d, He W-r, Kim C-N (2014b) Impacts of shape and height of upstream roof on airflow and pollutant dispersion inside an urban street canyon.
722 Environ Sci Pollut Res 22:2117-2137. https://doi.org/10.1007/s11356-014-3422-6
723 Huang Y-D, Hou R-W, Liu Z-Y, Song Y, Cui P-Y, Kim C-N (2019c) Effects of Wind Direction on the Airflow and Pollutant Dispersion inside a Long
724 Street Canyon. Aerosol Air Qual Res 19:1152-1171. https://doi.org/10.4209/aaqr.2018.09.0344
725 Huang Y-d, Ren S-q, Xu N, Luo Y, Sin CH, Cui P-Y (2021c) Impacts of specific street geometry on airflow and traffic pollutant dispersion inside a
726 street canyon. Air Quality, Atmosphere & Healthhttps://doi.org/10.1007/s11869-021-01101-y
727 Huang Y, Hu X, Zeng N (2009b) Impact of wedge-shaped roofs on airflow and pollutant dispersion inside urban street canyons. Build Environ
728 44:2335-2347. https://doi.org/10.1016/j.buildenv.2009.03.024
729 Jeanjean APR, Hinchliffe G, McMullan WA, Monks PS, Leigh RJ (2015b) A CFD study on the effectiveness of trees to disperse road traffic emissions
730 at a city scale. Atmos Environ 120:1-14. https://doi.org/10.1016/j.atmosenv.2015.08.003
731 Kastner-Klein P (1999) Description of wind – tunnel studies on flow field and dispersion characteristics in street canyons at the University of
732 Karlsruhe.
733 Li J, Niu J, Mak CM, Huang T, Xie Y (2018c) Assessment of outdoor thermal comfort in Hong Kong based on the individual desirability and
734 acceptability of sun and wind conditions. Build Environ 145:50-61. https://doi.org/10.1016/j.buildenv.2018.08.059
735 Li X, Liu C, Leung D (2005a) Development of a model for the determination of air exchange rates for street canyons. Atmos Environ 39:7285-7296.
736 https://doi.org/10.1016/j.atmosenv.2005.09.007
737 Li X, Liu C, Leung D, Lam K (2006) Recent progress in CFD modelling of wind field and pollutant transport in street canyons. Atmos Environ
738 40:5640-5658. https://doi.org/10.1016/j.atmosenv.2006.04.055
739 Liu C, Leung D, Barth M (2005b) On the prediction of air and pollutant exchange rates in street canyons of different aspect ratios using large-eddy
740 simulation. Atmos Environhttps://doi.org/10.1016/j.atmosenv.2004.08.036
741 Llaguno-Munitxa M, Bou-Zeid E, Hultmark M (2017c) The influence of building geometry on street canyon air flow: Validation of large eddy
742 simulations against wind tunnel experiments. J Wind Eng Ind Aerodyn 165:115-130. https://doi.org/10.1016/j.jweia.2017.03.007
743 Mei D, Wang Y, Deng Q (2017d) Modeling the Airflow and Particle Dispersion in Street Canyons under Unsteady Thermal Environment with
744 Sinusoidal Variation. Aerosol Air Qual Res 17:1021-1032. https://doi.org/10.4209/aaqr.2016.12.0559
745 Moonen P, Gromke C, Dorer V (2013a) Performance assessment of Large Eddy Simulation (LES) for modeling dispersion in an urban street canyon
746 with tree planting. Atmos Environ 75:66-76. https://doi.org/10.1016/j.atmosenv.2013.04.016
747 Moosavi L, Mahyuddin N, Ab Ghafar N, Azzam Ismail M (2014c) Thermal performance of atria: An overview of natural ventilation effective designs.
748 Renewable and Sustainable Energy Reviews 34:654-670. https://doi.org/10.1016/j.rser.2014.02.035
749 Muhsin F, Yusoff WFM, Mohamed MF, Sapian AR (2017e) CFD modeling of natural ventilation in a void connected to the living units of multi-
750 storey housing for thermal comfort. Energy Build 144:1-16. https://doi.org/10.1016/j.enbuild.2017.03.035
751 Pani SK, Lin N-H, RavindraBabu S (2020d) Association of COVID-19 pandemic with meteorological parameters over Singapore. Sci Total Environ
752 740:140112. https://doi.org/10.1016/j.scitotenv.2020.140112
753 Reiminger N, Vazquez J, Blond N, Dufresne M, Wertel J (2020e) CFD evaluation of mean pollutant concentration variations in step-down street
754 canyons. J Wind Eng Ind Aerodyn 196:104032. https://doi.org/10.1016/j.jweia.2019.104032
755 Ricci A, Burlando M, Repetto MP, Blocken B (2019d) Simulation of urban boundary and canopy layer flows in port areas induced by different marine
756 boundary layer inflow conditions. Sci Total Environ 670:876-892. https://doi.org/10.1016/j.scitotenv.2019.03.230
757 Roth M, Chow WTL (2012c) A historical review and assessment of urban heat island research in Singapore. Singapore Journal of Tropical Geography
758 33:381-397. https://doi.org/10.1111/sjtg.12003
759 Salim SM, Buccolieri R, Chan A, Di Sabatino S (2011b) Numerical simulation of atmospheric pollutant dispersion in an urban street canyon:
760 Comparison between RANS and LES. J Wind Eng Ind Aerodyn 99:103-113. https://doi.org/10.1016/j.jweia.2010.12.002

761 Salim SM, Cheah SC, Chan A (2011c) Numerical simulation of dispersion in urban street canyons with avenue-like tree plantings: Comparison
762 between RANS and LES. Build Environ 46:1735-1746. https://doi.org/10.1016/j.buildenv.2011.01.032
763 Sanchez B, Santiago JL, Martilli A, Martin F, Borge R, Quaassdorff C, de la Paz D (2017f) Modelling NOX concentrations through CFD-RANS in an
764 urban hot-spot using high resolution traffic emissions and meteorology from a mesoscale model. Atmos Environ 163:155-165.
765 https://doi.org/10.1016/j.atmosenv.2017.05.022
766 Tominaga Y, Stathopoulos T (2011d) CFD modeling of pollution dispersion in a street canyon: Comparison between LES and RANS. J Wind Eng Ind
767 Aerodyn 99:340-348. https://doi.org/10.1016/j.jweia.2010.12.005
768 Vranckx S, Vos P, Maiheu B, Janssen S (2015c) Impact of trees on pollutant dispersion in street canyons: A numerical study of the annual average
769 effects in Antwerp, Belgium. Sci Total Environ 532:474-483. https://doi.org/10.1016/j.scitotenv.2015.06.032
770 Weerasuriya AU, Zhang X, Lu B, Tse KT, Liu C-H (2020f) Optimizing Lift-up Design to Maximize Pedestrian Wind and Thermal Comfort in 'Hot-
771 Calm' and 'Cold-Windy' Climates. Sustainable Cities and Society 58:102146. https://doi.org/10.1016/j.scs.2020.102146
772 Xu H, Yan C, Fu Q, Xiao K, Yu Y, Han D, Wang W, Cheng J (2020g) Possible environmental effects on the spread of COVID-19 in China. Sci Total
773 Environ 731:139211. https://doi.org/10.1016/j.scitotenv.2020.139211
774 Yang W, Wong NH, Jusuf SK (2013b) Thermal comfort in outdoor urban spaces in Singapore. Build Environ 59:426-435.
775 https://doi.org/10.1016/j.buildenv.2012.09.008
776 Yim SHL, Fung JCH, Lau AKH, Kot SC (2010) Corrigendum to "Air ventilation impacts of the "wall effect" resulting from the alignment of high-
777 rise buildings" [Atmos. Environ. 43 (2009) 4982–4994]. Atmos Environ 44:1367. https://doi.org/10.1016/j.atmosenv.2010.01.013
778 Zhang X, Tse KT, Weerasuriya AU, Kwok KCS, Niu J, Lin Z, Mak CM (2018d) Pedestrian-level wind conditions in the space underneath lift-up
779 buildings. J Wind Eng Ind Aerodyn 179:58-69. https://doi.org/10.1016/j.jweia.2018.05.015
780 Zhang Y, Gu Z, Yu CW (2018e) Review on Numerical Simulation of Airflow and Pollutant Dispersion in Urban Street Canyons under Natural
781 Background Wind Condition. Aerosol Air Qual Res 18:780-789. https://doi.org/10.4209/aaqr.2017.09.0303

Figures

Figure 1

(a) Street canyon configuration; **(b)** Pedestrian respiration planes on both sides of the canyon and location of the four line sources placed on the street floor

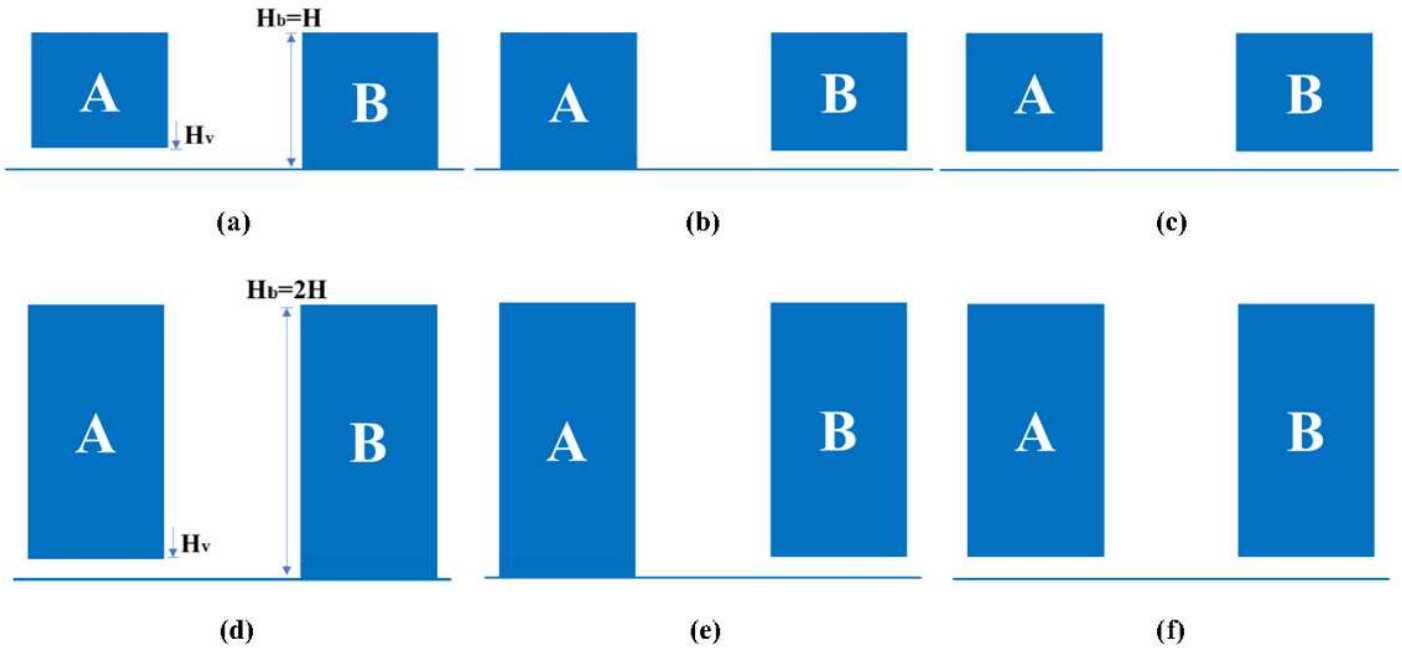

Figure 2

Sketches of the cross-section of the street canyons with void deck; **(a)** Leeward side & $H_b/W=1$; **(b)** Windward side & $H_b/W=1$; **(c)** Both side & $H_b/W=1$; **(d)** Leeward side & $H_b/W=2$; **(e)** Windward side & $H_b/W=2$; **(f)** Both side & $H_b/W=2$

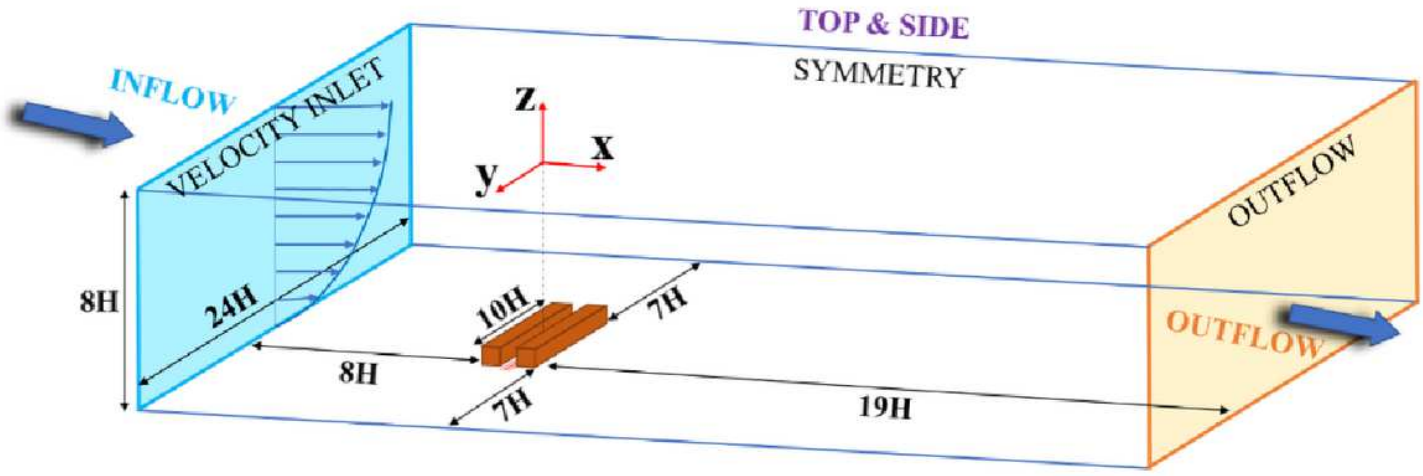

Figure 3

Sketches of the computational domain and boundary conditions

Figure 4

Grid independence analysis; **(a)** Leeward wall; **(b)** Windward wall

Figure 5

Comparisons of K along three vertical lines on the canyon walls between WT measurement and numerical results; **(a)** Leeward wall; **(b)** Windward wall

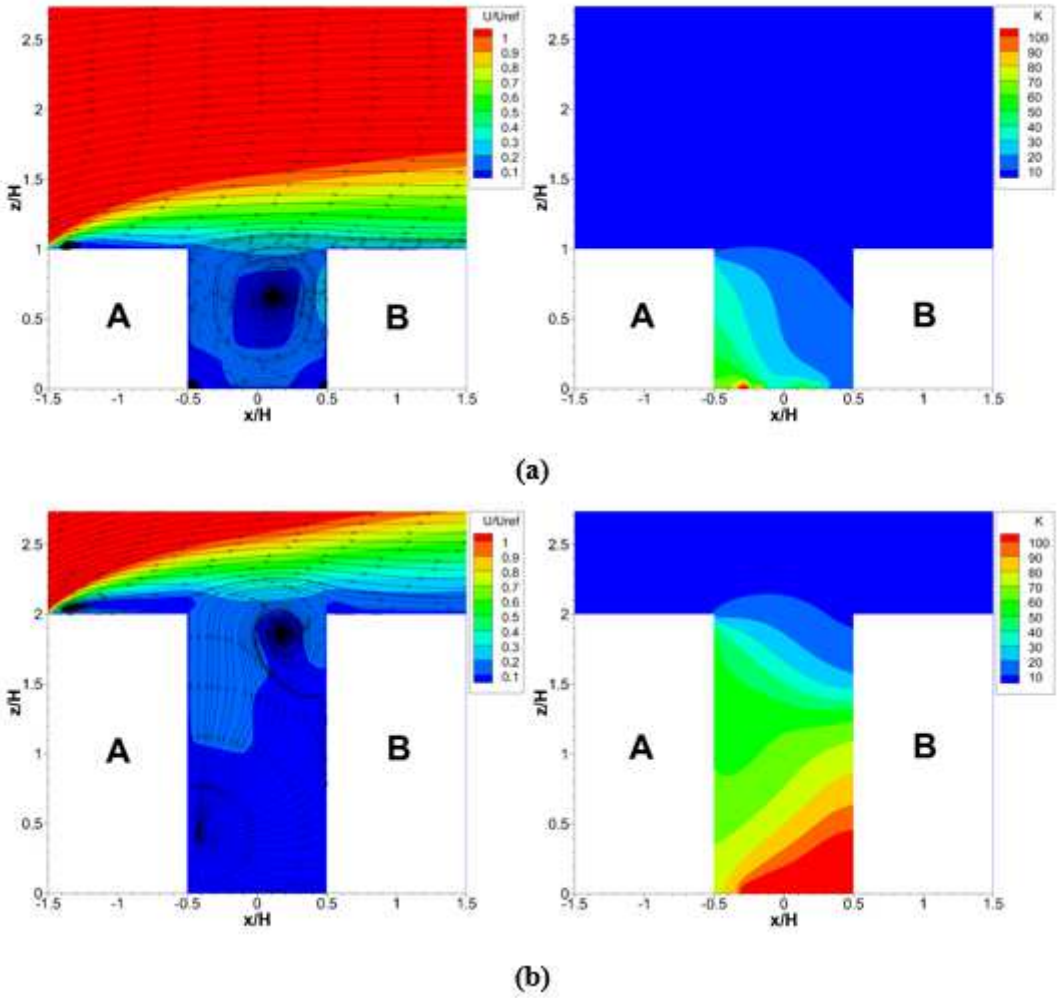

Figure 6

Airflow (streamlines and normalized velocity magnitude contours) and dimensionless *K* pattern on the vertical central plane of the regular canyons; **(a)** $H_b/W=1$; **(b)** $H_b/W=2$

Figure 7

Airflow and dimensionless pollutant concentration pattern on the vertical central plane of the canyons ($H_b/W=1$) with different locations and heights of void deck; **(a)** Leeward side & $H_v/W=1/6$; **(b)** Leeward side & $H_v/W=1/4$; **(c)** Windward side & $H_v/W=1/6$; **(d)** Windward side & $H_v/W=1/4$; **(e)** Both sides & $H_v/W=1/6$; **(f)** Both sides & $H_v/W=1/4$

Figure 8

Airflow and dimensionless pollutant concentration pattern on the vertical central plane of the canyons ($H_b/W=2$) with different locations and heights of void deck; **(a)** Leeward side & $H_v/W=1/6$; **(b)** Leeward side & $H_v/W=1/4$; **(c)** Windward side & $H_v/W=1/6$; **(d)** Windward side & $H_v/W=1/4$; **(e)** Both side & $H_v/W=1/6$; **(f)** Both side & $H_v/W=1/4$

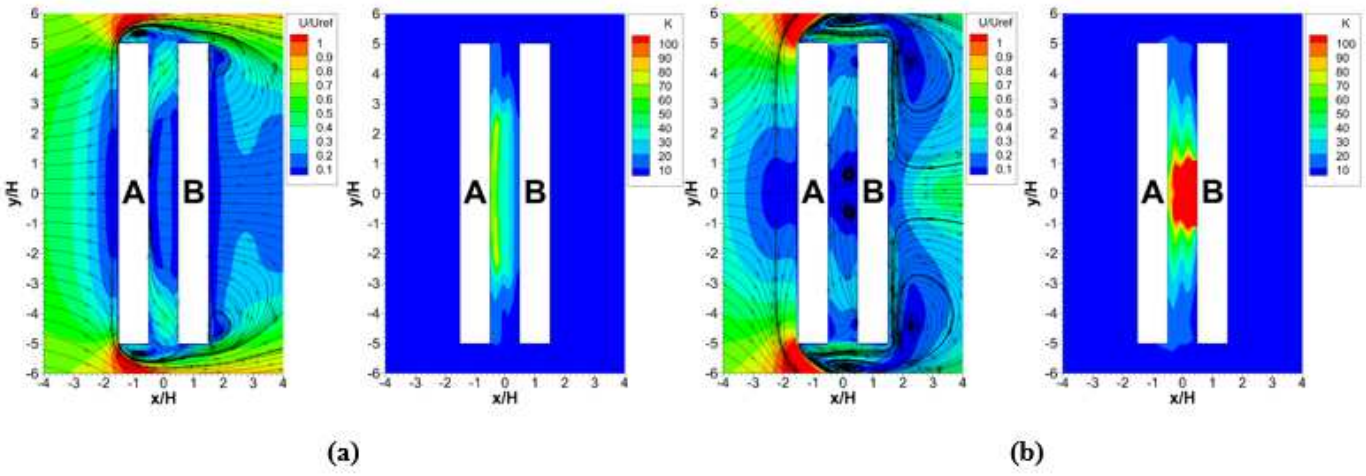

Figure 9

Airflow and pollutant concentration distribution at the pedestrian respiration height of the regular canyons; **(a)** $H_b/W=1$; **(b)** $H_b/W=2$

Figure 10

Airflow and pollutant concentration distribution at the pedestrian respiration height of the canyons ($H_b/W=1$) with different locations and heights of void deck; **(a)** Leeward side & $H_v/W=1/6$; **(b)** Leeward side & $H_v/W=1/4$; **(c)** Windward side & $H_v/W=1/6$; **(d)** Windward side & $H_v/W=1/4$; **(e)** Both side & $H_v/W=1/6$; **(f)** Both side & $H_v/W=1/4$

Figure 11

Airflow and pollutant concentration distribution at the pedestrian respiration height of the canyons ($H_b/W=2$) with different locations and heights of void deck; **(a)** Leeward side & $H_v/W=1/6$; **(b)** Leeward side & $H_v/W=1/4$; **(c)** Windward side & $H_v/W=1/6$; **(d)** Windward side & $H_v/W=1/4$; **(e)** Both side & $H_v/W=1/6$; **(f)** Both side & $H_v/W=1/4$

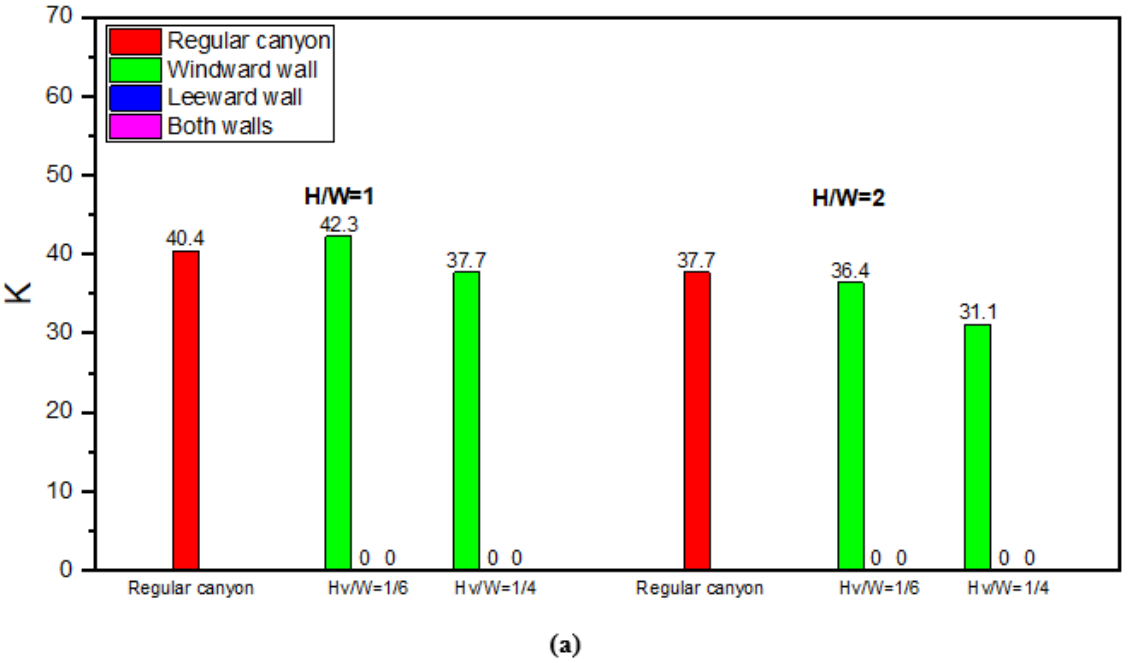

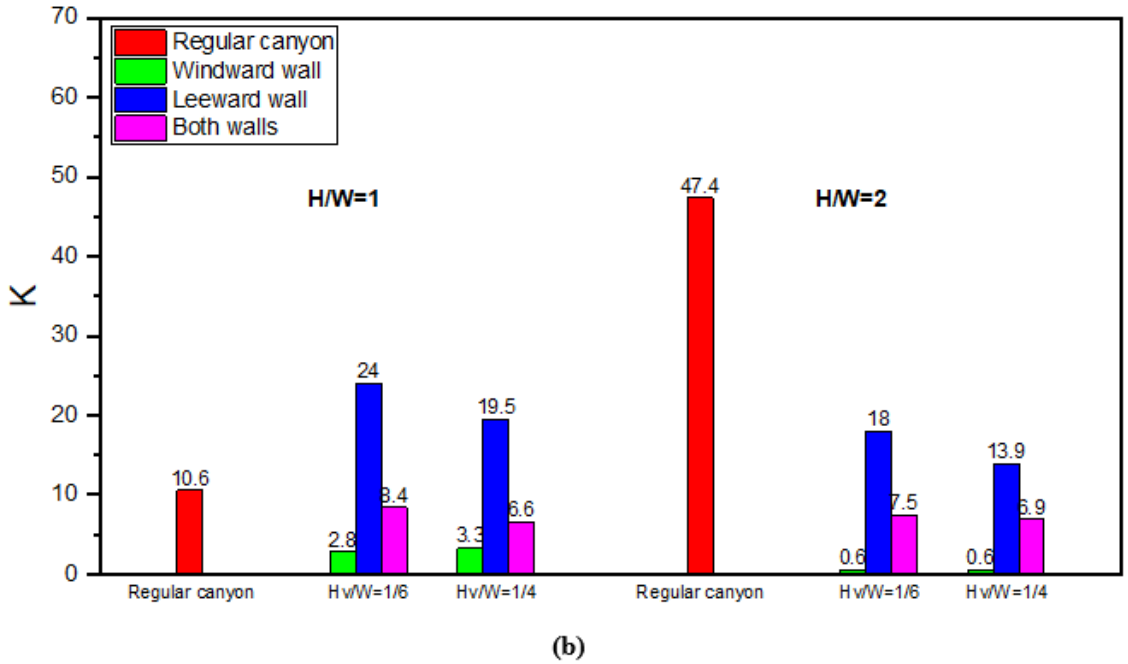

Figure 12

Mean dimensionless pollutant concentrations at the pedestrian respiration planes of the fourteen different street configurations; **(a)** Leeward side; **(b)** Windward side

Figure 13

Dimensionless pollutant concentration patterns on the leeward wall (A) and windward wall (B) of the regular street canyons; **(a)** $H_b/W=1$; **(b)** $H_b/W=2$

Figure 14

Dimensionless pollutant concentration patterns on the leeward wall (A) and windward wall (B) of the canyons ($H_b/W=1$) with different locations and heights of void deck; **(a)** Leeward side & $H_v/W=1/6$; **(b)** Leeward side & $H_v/W=1/4$; **(c)** Windward side & $H_v/W=1/6$; **(d)** Windward side & $H_v/W=1/4$; **(e)** Both side & $H_v/W=1/6$; **(f)** Both side & $H_v/W=1/4$

Figure 15

Dimensionless pollutant concentration patterns on the leeward wall (A) and windward wall (B) of the canyons ($H_b/W=2$) with different locations and heights of void deck; **(a)** Leeward side & $H_v/W=1/6$; **(b)** Leeward side & $H_v/W=1/4$; **(c)** Windward side & $H_v/W=1/6$; **(d)** Windward side & $H_v/W=1/4$; **(e)** Both side & $H_v/W=1/6$; **(f)** Both side & $H_v/W=1/4$

Figure 16

Mean *K* on the canyon walls of the fourteen different street configurations; **(a)** Leeward wall; **(b)** Windward wall

Supplementary Files

This is a list of supplementary files associated with this preprint. Click to download.

- tables.docx